Environ. Sci. Technol. **2010,** *44,* 349–355

Dissolution Potential of SO_2 Co-Injected with CO_2 in Geologic Sequestration

LAUREN E. CRANDELL, BRIAN R. ELLIS, AND CATHERINE A. PETERS*

Department of Civil & Environmental Engineering, Princeton University, Princeton, New Jersey 08540

Received August 27, 2009. Revised manuscript received November 19, 2009. Accepted November 20, 2009.

Sulfur dioxide is a possible co-injectant with carbon dioxide in the context of geologic sequestration. Because of the potential of SO_2 to acidify formation brines, the extent of SO_2 dissolution from the CO_2 phase will determine the viability of co-injection. Pressure-, temperature-, and salinity-adjusted values of the SO_2 Henry's Law constant and fugacity coefficient were determined. They are predicted to decrease with depth, such that the solubility of SO_2 is a factor of 0.04 smaller than would be predicted without these adjustments. To explore the potential effects of transport limitations, a nonsteady-state model of SO_2 diffusion through a stationary cone-shaped plume of supercritical CO_2 was developed. This model represents an end-member scenario of diffusion-controlled dissolution of SO_2, to contrast with models of complete phase equilibrium. Simulations for conditions corresponding to storage depths of 0.8−2.4 km revealed that after 1000 years, 65−75% of the SO_2 remains in the CO_2 phase. This slow release of SO_2 would largely mitigate its impact on brine pH. Furthermore, small amounts of SO_2 are predicted to have a negligible effect on the critical point of CO_2 but will increase phase density by as much as 12% for mixtures containing 5% SO_2.

Introduction

Geologic sequestration of carbon dioxide is emerging as a promising carbon mitigation strategy (*1*−*3*). Electric power plants, which are the largest point sources from which CO_2 will be captured, emit other important pollutants such as sulfur dioxide, and there is the possibility that such pollutants could be disposed of by co-injection with CO_2 into deep geologic formations. Every year, the electric power industry collectively spends more than $5 billion on permits for the right to emit SO_2 (*4*). Given the environmental and human health benefits of controlling SO_2 emissions (*5*), it may be economically advantageous to dispose of SO_2 with CO_2. However, the effects that impurities in the CO_2 stream will have on injection and long-term storage are largely unknown. Regulations governing the injection of CO_2 have been proposed by the U.S. EPA; however, there has been no specification of the required purity of the injected stream except that it must not meet the definition of a hazardous waste (*6*). John Gale, of the IEA, recently commented on the need to understand the effects of impurities on capture, transport, and storage before setting purity regulations (*7*).

* Corresponding author. Tel: 609-258-5645; E-mail: cap@princeton.edu.

In aqueous solution, SO_2 may form sulfurous acid, sulfuric acid, and even H_2S (*8*). With the exception of H_2S, these are acids stronger than carbonic acid, formed from aqueous CO_2. Acidity in the context of geologic CO_2 sequestration will accelerate mineral dissolution and precipitation, which may affect formation porosity and permeability, integrity of wellbore cements, and caprock integrity (*9*−*13*). Gunter et al. (*11*) examined water-rock reactions for injection streams of CO_2, H_2SO_4, and H_2S and predicted that these acids could be effectively buffered by the formation mineralogy, thus reducing the potential for long-term brine acidification. However, other geochemical modeling studies (*14*−*16*) predict that storage of sulfur co-injectants with CO_2 would create persistent, highly acidic conditions. Knauss et al. (*15*) used a reactive transport simulation and predicted that even small amounts of SO_2, such as 10^{-6} bar partial pressure, would create pH conditions near unity. Under these acidic conditions, porosity will be increased because of mineral dissolution and carbonate mineral precipitation will be inhibited. Similarly, Xu et al. (*16*) predicted that co-injection of SO_2 would create a larger and more acidic zone than injection of CO_2 alone and would increase porosity in the acidic zone due to mineral dissolution and decrease porosity at the acid front due to sulfate precipitation.

The magnitude of brine acidification will depend on the extent and rate of dissolution of SO_2 out of the injected CO_2. One of the objectives of this work was to determine a means of predicting the solubility of SO_2 in formation brines under geologic sequestration conditions. Solubility of CO_2 under these conditions has been fairly well examined (*17*−*19*); however, little is known of SO_2 solubility at high temperature, pressure, and salinity conditions. At injection depths below 800 m, where CO_2 would exist as a supercritical fluid (*20*), temperatures are greater than 30 °C, and pressures are greater than 74 bar. The solubility of SO_2 in pure water has been determined at temperatures up to 130 °C, but at pressures up to only 25 bar (*21*−*23*). Furthermore, at depths relevant for geologic sequestration, brine salinity in sedimentary basins is as high as 225 g/L (approximately 3.8 M) (*20*). SO_2 solubility has been measured in 0.1−6 M NaCl solutions (*24*−*26*), and in mixed electrolyte solutions (*27*−*29*) but not at the pressures relevant for geologic sequestration.

In this work, we present a means of determining the phase partitioning of SO_2 from supercritical CO_2 ($scCO_2$) by using pressure-, temperature-, and salinity-adjusted parameters including the Henry's Law constant and the CO_2-phase fugacity coefficient. We examine how these parameters and the resulting SO_2 brine concentrations would vary with depth, in comparison to CO_2 concentrations. Additionally, densities of CO_2−SO_2 mixtures under relevant pressure and temperature (*PT*) conditions, along with mixture critical points, are calculated. These properties are important to demonstrate the effects of SO_2 additives on CO_2 injection depth and migration potential. Finally, the diffusivity of SO_2 in $scCO_2$ is estimated, and its variation with depth and *PT* conditions is examined.

In addition to the need to quantify the potential for equilibrium phase partitioning of SO_2, there is a need to estimate the flux of SO_2 from the injected CO_2 to the bulk brine phase. Previous modeling studies (*15, 16*) of co-injection of SO_2 with CO_2 assume sustained phase equilibrium between all the $scCO_2$ and brine. This is an extreme case scenario in which there is no limitation on contact of SO_2 with the brine. The opposite extreme case is a scenario in which SO_2 is limited by diffusion through a stationary $scCO_2$ phase. These two extremes bound reality in which the actual rate of SO_2 contact

10.1021/es902612m
Published on Web 12/09/2009

with brine is controlled by process complexities and system heterogeneities.

To address the need to understand the diffusion-limited bounding scenario, the second major objective of this work was to describe diffusion-limited dissolution behavior of SO_2 into brines in the context of co-injection with CO_2 in geologic sequestration. A nonsteady-state model of SO_2 diffusion through a stationary cone-shaped plume of $scCO_2$ was developed and used to simulate fluxes of SO_2 into the brine outside the $scCO_2$ plume. Pressure- and temperature-adjusted binary diffusion coefficients of SO_2 in $scCO_2$ were estimated. A variety of depths were considered to determine how changes in temperature and pressure affect the properties. Two different mixture compositions, 1 and 5% SO_2, were considered, corresponding to moderate-to-high ratios of SO_2 to CO_2 in emissions from electric power plants.

Methods

CO_2−SO_2 Mixture Properties. Critical points for mixtures of CO_2 and SO_2 were estimated by using the corresponding states method as given by Lee and Kesler (*30*). Yang et al. (*31*) examined the accuracy of this method in describing CO_2 mixtures and concluded that Lee−Kesler type equations of state are as accurate, sometimes more so, than more complex cubic equations of state. This estimation used values of the pure component critical molar volumes, critical temperatures, and acentric factors from reported data (*31*−*34*) (Supporting Information, Table S1).

The densities of mixtures of CO_2 and SO_2 were estimated by using the method given in Lee and Kesler (*30*). For consistency, this method was also used to estimate the densities of pure CO_2 despite the availability of CO_2 equations of state (*35*). Densities were calculated at *PT* conditions corresponding to a variety of depths, based on gradients from reported data (*36, 37*) as described in the Supporting Information (Section S-1).

Partitioning into Brine. For the case of phase equilibrium partitioning of SO_2 between $scCO_2$ and brine, the convention of the infinite-dilution reference state for the aqueous phase is adopted. This results in an expression relating the SO_2 concentration in the brine phase, C[M], to the partial pressure in the $scCO_2$ phase, P_{SO2} [atm]:

$$C = \phi_{SO2} P_{SO2} K_H \tag{1}$$

where ϕ_{SO2} is the fugacity coefficient of SO_2 in the $scCO_2$ phase and K_H is the Henry's Law constant in [M/atm].

The adjustment of the Henry's Law constant for high pressures was done by using the Krichevsky−Ilinskaya equation, which also adjusts for variation in activity coefficient, important for highly soluble gases (*38*). This equation relates the Henry's law constant, $K_{H,P}$, at system pressure, P, to the Henry's law constant at a lower reference pressure, K_{H,P^*}, through

$$\ln K_{H,P} = \ln K_{H,P^*} - \frac{A}{RT}(x_j^2 - 1) - \frac{\bar{v}^{\infty}_{SO2}(P - P^*)}{RT} + \ln\left(\frac{\bar{V}_{P^*}}{\bar{V}_P}\right) \tag{2}$$

where A is the Margules constant, x_j is the mole fraction of water in the brine phase, $\bar{v}^{\infty}_{SO2}$ is the partial molar volume of SO_2 at infinite dilution, P^* is the reference pressure, R is the universal gas constant, T is the temperature, and $\bar{V}_P$ is the molar volume of water. In this work, the last term is ignored because changes in the molar volume of water with pressure are assumed negligible. Henry's Law constants for SO_2 at P^* of 1 bar were taken from Rabe and Harris (*21*) for several temperatures representative of geologic sequestration conditions (given in Table S2 in the Supporting Information).

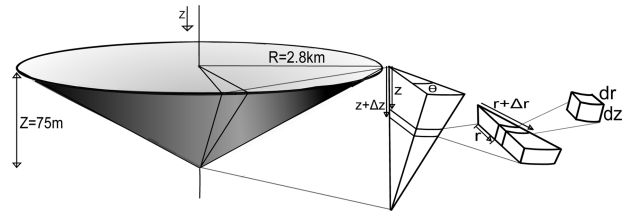

FIGURE 1. Diagram of model injection plume showing an example differential volume element.

These values of $K_{H,P}$* refer to aqueous SO_2 in the unreacted form, as opposed to the total SO_2 in solution. Partial molar volumes of SO_2 at infinite dilution (Table S1 in the Supporting Information) were taken from Brelvi and O'Connell (*39*). The Margules constants were estimated via regression of measurements of SO_2 solubility in pure water at pressures up to 11 bar (*22*).

The Henry's Law constants were adjusted for saline conditions by using the Schumpe model (*27*) for mixed electrolyte solutions with an adjusted gas-specific parameter given by Rodriguez-Sevilla et al. (*24*). A 1 M NaCl solution was selected to represent the brine.

The fugacity coefficient for SO_2 in the $scCO_2$ was determined from the second virial coefficients, determined from the reduced-virial-coefficient method in Tarakad and Danner (*40*).

SO_2 Diffusivity in $scCO_2$. The diffusion coefficient for SO_2 in $scCO_2$, $D_{SO2,CO2}$ at high pressures was estimated by using the Takahashi correlation (*41*) as described in the Supporting Information (Section S-4). Values of $D_{SO2,CO2}$ at relevant conditions are also given in the Supporting Information (Section S-4).

Model System and Simplifications. A model system was conceptualized to represent an extreme-end-member scenario in which SO_2 contact with the bulk brine is entirely diffusion-limited within the $scCO_2$ phase. By "bulk brine", we refer to the brine phase outside the $scCO_2$ plume. The system is a $scCO_2$ phase within a geologic formation after the injection period (Figure 1). We selected a cone as simplified geometry to mimic the shape of a CO_2 plume trapped underneath a caprock seal. For simplicity, the $scCO_2$ is assumed to be stationary. During the injection process, pressure will force the CO_2 to flow into the formation (see e.g refs *42*−*44*). Post-injection, however, these pressures will dissipate, and CO_2 flow will be slower, driven only by buoyancy override and hydrodynamic flow. Furthermore, in deep aquifers, the flow of water is slow, 1−10 cm/yr (*45*), which means that hydrodynamic forces are minimal.

The other type of CO_2 flow, which is not considered here, is the flow driven by the new density gradients that will be created because of spatial differences in SO_2 concentrations within the $scCO_2$ phase. A circulation pattern may emerge in which SO_2-rich CO_2 near the top, center of the cone will exchange with the less dense CO_2 that is depleted of SO_2. (Note that this does not affect mixing between the brine phase and the $scCO_2$ phase because the density of the SO_2-rich $scCO_2$ phase is still significantly less than the density of the brine phase.) This advective transport is one of the processes that will enhance SO_2 flux relative to the extreme case of diffusion in a stagnant fluid, modeled here.

Another process not considered is partitioning of SO_2 into residual brine trapped within the volume of the cone. Partitioning to residual brine may be significant. The effect, relative to what is modeled here, is that the diffusive flux to the bulk brine would be diminished because of the reduced SO_2 concentrations in the $scCO_2$ phase.

A cone volume of 6.1×10^8 m^3 was calculated on the basis of a CO_2 density of 750 kg/m^3, an aquifer porosity of 20%, and a 50 year injection period at a rate of 1.83 Mton/year

(*46*). By assuming a formation thickness of 75 m and by assuming that the height of the cone equals this thickness, a cone with the selected injection volume would extend to a radius of 2.8 km.

SO_2 Diffusion Modeling. The cone radius was discretized in radial coordinates by first dividing it into wedges with angle θ. The wedges with total height Z were divided into slices with thickness Δz. Slices were then divided into segments with width Δr, as shown in Figure 1. The derivation of the equation for diffusive mass transport of SO_2 in $scCO_2$ in a differential volume element is presented in detail in the Supporting Information (Section S-5). The resulting model equation is

$$\frac{\partial C}{\partial t} = D_{\text{eff}}\left(\frac{1}{r}\frac{\partial C}{\partial r} + \frac{\partial^2 C}{\partial r^2} + \frac{\partial^2 C}{\partial z^2}\right) \quad (3)$$

where C is the concentration of SO_2 and D_{eff} is the effective diffusion coefficient. The effective diffusion coefficient is calculated from $D_{SO2,CO2}$, formation porosity, n, and tortuosity, σ (*47*).

$$D_{\text{eff}} = D_{SO2,CO2}\frac{n}{\sigma} \quad (4)$$

For this work, tortuosity was selected as $\sigma = 2$ to represent high diffusive flux.

The initial condition assumes a spatially uniform concentration of 1 or 5% SO_2, within the $scCO_2$. A no-flux boundary was assumed at the top of the cone, representing an aquifer bounded by an impermeable caprock. Diffusion within the cone is driven by a concentration gradient created by preferential dissolution of SO_2 into the bulk brine at the cone boundary. SO_2 dissolution was predicted by using eq 1 and the estimated Henry's Law constant and fugacity coefficient. The model does not account for dissolution of CO_2. In Ellis et al. (*8*), we describe this process and examine the change in the $scCO_2$ plume size by considering different scenarios for brine-phase transport. To create a maximum driving force for dissolution, at each time step, the brine at the cone boundary was reset to have a zero concentration of SO_2. This is a realistic condition because dissolved SO_2 will quickly convert to acid reaction products (see Ellis et al. (*8*)). The diffusion equation was numerically solved by using a time-split explicit difference method as described in the Supporting Information (Section S-5).

Results and Discussion

CO_2–SO_2 Mixtures. The critical points estimated for mixtures of CO_2 and SO_2 are shown in the phase diagram in Figure 2. For reference, gas–liquid phase boundaries for pure CO_2 and SO_2 are also shown. (Published correlations were used for the phase boundaries for CO_2 (*48*) and SO_2 (*34*).) Whereas the critical temperature of SO_2 is much higher than that of CO_2, pure SO_2 and pure CO_2 have similar critical pressures. Also, critical points for mixtures of SO_2 and CO_2 are predicted to be fairly constant in pressure. This implies that, in the context of injection, to ensure a supercritical mixture, less than an additional 1 m depth is required for 1% SO_2 mixtures and an additional 3.5 m for 5% SO_2 mixtures.

Estimated densities are shown in Figure 3, along a trajectory corresponding to a surface temperature of 10 °C. Uncertainties are 5.3% (see Supporting Information). The density of pure CO_2 ranges from 754 to 759 kg/m^3 from depths of 0.8 to 2.4 km (Figure 3a). This variation is small because, coincidentally, the *PT* depth trajectory is closely aligned with an iso-density (isopycnic) line in the supercritical regime. Densities of mixtures of CO_2 and SO_2 (Figure 3b,c) are larger than those of pure CO_2. For the conditions of interest, densities are up to 3% larger for 1% SO_2 mixtures and up to 12% larger for 5% SO_2 mixtures. This increase is expected

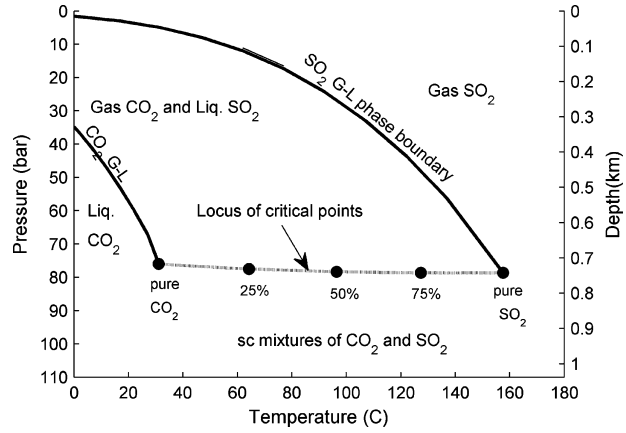

FIGURE 2. Pressure–temperature phase diagram for CO_2, SO_2, and their mixtures. Gas–liquid (G-L) phase boundaries are shown for the pure substances, along with the locations of critical points for mixtures of CO_2 and SO_2. The diagram is inverted, showing pressure decreasing on the left ordinate axis to correspond to variation with depth, depicted on the right ordinate axis.

given the larger density of pure SO_2. For pressures and temperatures that correspond to depths between 0.8 and 2.4 km, the density of SO_2, as measured by Ihmels (*49*), ranges from 1373 to 1300 kg/m^3. Thus, small amounts of SO_2 have a large effect on the mixture density. In the context of geologic sequestration, this may be beneficial. The densities of brines vary from 950 to 1200 kg/m^3 (*50*). A decrease in the density difference between the two phases would decrease the buoyancy of $scCO_2$ and may decrease leakage potential.

Equilibrium Partitioning of SO_2 into Brine. Salinity-adjusted values of the Henry's Law constant for SO_2 were determined at 20, 40, 60, and 70 °C, for pressures from 1 to 260 bar, corresponding to depths up to 2.4 km. These values have estimated errors of 14% (see Supporting Information). For example, at 1.2 km depth, the Henry's Law constant is predicted to be 0.58 ± 0.08 M/atm. Interpolations of the computed values are shown as contours in a *PT* plot in the Supporting Information (Section S-6). Values of K_{H,P^*} decrease with temperature and pressure. Therefore, the Henry's Law constant decreases with increasing injection depth such that SO_2 solubility at geologic sequestration conditions is less than that under conditions at the land surface (value given in Table S1 in the Supporting Information).

The depth variations of all the factors that govern SO_2 equilibrium phase partitioning into brine (eq 1) are shown in Figure 4. Partial pressure increases linearly with depth, but ϕ_{SO2} and K_H decrease nonlinearly. At shallow depths, SO_2 would behave ideally in the CO_2 phase, with ϕ_{SO2} approximately equal to unity, and at greater depths, substantial negative deviations from ideality are predicted. Also shown in Figure 4 is the resulting molar concentration of SO_2 in brine and its variation with depth. This was computed with the simplifying assumptions that, over the entire depth, the aqueous phase is a 1 M NaCl brine, and the brine is in equilibrium with $scCO_2$ containing 1 or 5% of SO_2. Also, this calculation does not account for the fact that phase partitioning of a finite mass of SO_2 would deplete it from the $scCO_2$ phase, and the resulting concentration of SO_2 in the brine would be much smaller than what is computed here. (This more realistic case is considered in Ellis et al. 2009 (*8*).) However, this simplified case is examined for the sake of illustration. At land-surface conditions of 1 bar and 10 °C, the solubility of SO_2 would be 0.02 M for 1% SO_2 and 0.09 M for 5% SO_2. As depth increases, the increase in partial pressure causes phase partitioning to increase by one-to-two orders of magnitude to a maximum of 0.45 M at 0.8 km

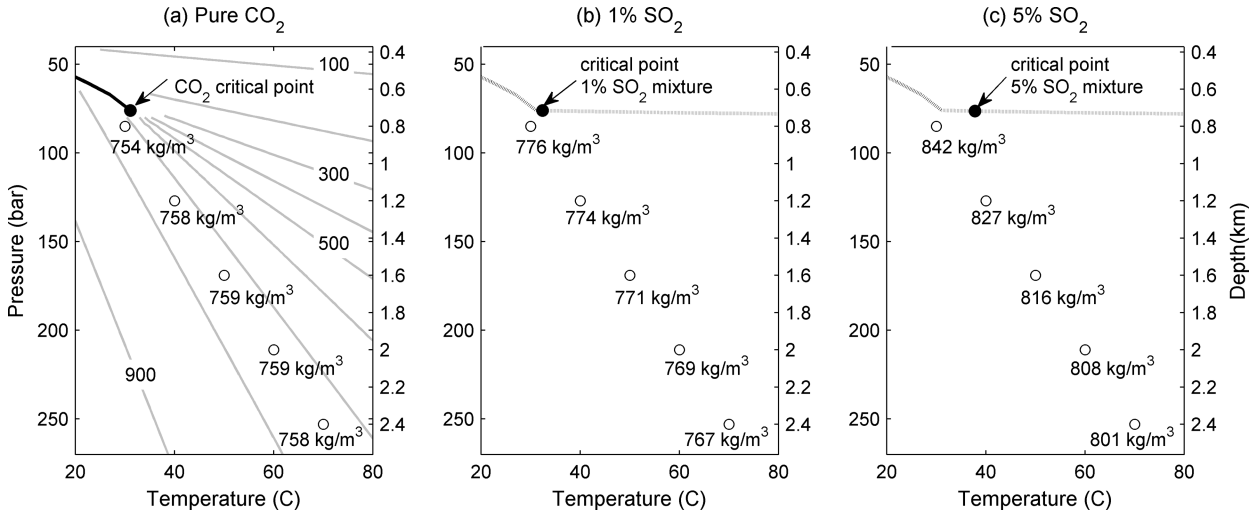

FIGURE 3. Densities of pure CO_2 (a) and mixtures of 1% (b) and 5% (c) SO_2 with CO_2 along a *PT* trajectory corresponding to a pressure gradient of 105 bar/km and a temperature gradient of 25 °C/km, with a surface temperature of 10 °C. Contours in (a) correspond to constant densities of pure CO_2 in kg/m^3.

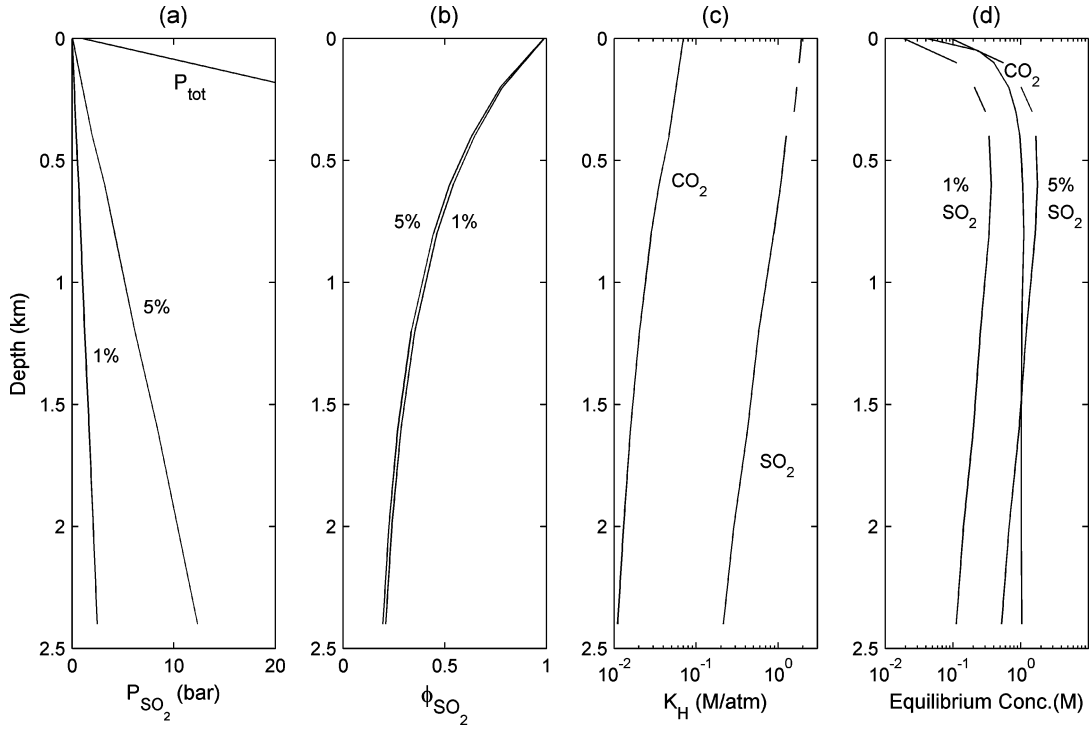

FIGURE 4. (a–c) Variation with depth of the factors that determine phase partitioning between $scCO_2$ and 1 M NaCl brine and (d) resulting brine-phase concentrations.

for 1% SO_2 and 2.2 M at 0.6 km for 5% SO_2. At greater depths, the effects of increasing nonideality in the $scCO_2$ phase and decreasing Henry's Law constant reverse the trend, causing the phase partitioning of SO_2 to decrease with depth.

SO_2-phase partitioning can be compared with the solubility of CO_2 by using the values calculated by Duan and Sun (*18*). A major difference between the two cases is that SO_2 is a minor mixture component with significant nonideal solution behavior and CO_2 is a nearly pure component with less extreme deviations from ideality. Consequently, the value of ϕ is not as important for CO_2 as it is for SO_2. At *PT* conditions representative of the land surface, the solubility of CO_2 in 1 M NaCl is 0.04 M, and it increases by two orders of magnitude to a value of 1.06 M at a depth of 1.2 km (Figure 4d). This similarity to our findings for SO_2 at shallow depths is expected because the determining factor is the change in pressure. Beyond a depth of 1.2 km, the solubility of CO_2 levels off (Figure 4d), which is explained mostly by the increasing importance of the Henry's Law constant. By using the K_H correlations presented by Bachu and Adams (*17*) and correcting them for salinity by using the Schumpe model (*27*), the pressure-adjusted Henry's Law constants for CO_2 were calculated. These values were found to decrease from 0.053 M/atm at the surface to 0.009 M/atm at a depth of 2.4 km (Figure 4c). In comparison with SO_2, values of $K_{H,P}$ for CO_2 are always smaller, reflecting the higher aqueous solubility of SO_2. In fact, the solubility of SO_2 is so much higher that its concentration in the brine phase is comparable to that of CO_2 despite the fact the mole fraction of SO_2 is so small. At 1.2 km, the equilibrium concentration in the brine

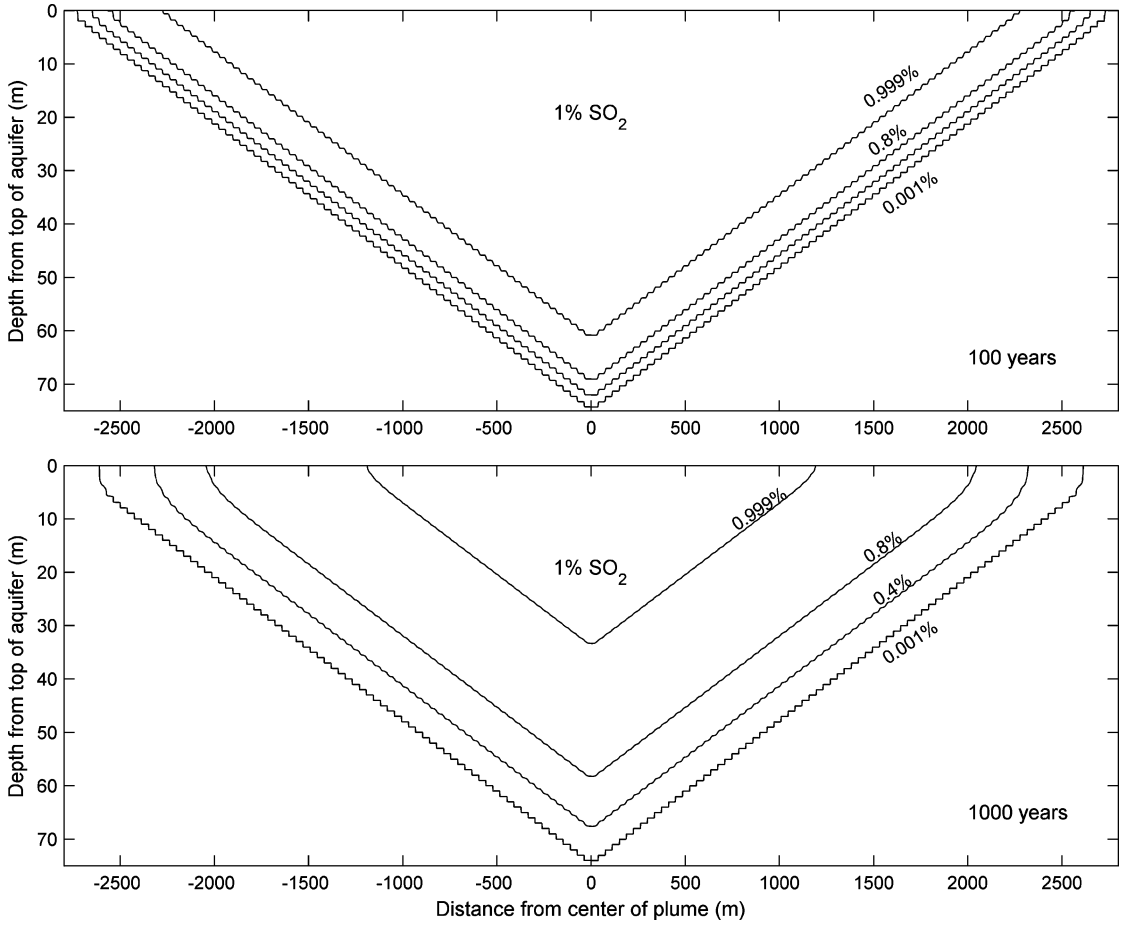

FIGURE 5. Concentration contours for SO_2 within the model $scCO_2$ cone after 100 and 1000 years for the case of an initial condition of 1% SO_2, temperature of 40 °C, and pressure of 127 bar corresponding to a depth of 1.2 km. The phase boundary between $scCO_2$ and brine is coincident with the 0.001% line.

is 0.38 and 1.8 M for 1 and 5% SO_2, respectively and 1.03 M for CO_2 at 1.2 km (Figure 4d).

SO_2 Diffusion through $scCO_2$. The predicted diffusion of SO_2 through the model $scCO_2$ cone is shown in Figure 5, for the case of 1% SO_2, as concentration profiles through a vertical section of the cone. The concentration of SO_2 near the cone boundary decreases early on because of the relatively high solubility of SO_2 in the bulk brine. The resulting depletion of SO_2 at this boundary creates a concentration gradient within the $scCO_2$ that causes diffusive flux of SO_2 from the center of the plume. The simulations predict that the concentration contours are roughly parallel with the cone boundary. The parallel contours establish a "zone of depletion" of fairly uniform thickness at the boundary of the cone. If we arbitrarily define the zone of depletion to be bounded by where the SO_2 concentration equals 0.999%, after 100 years, it is 15 m thick, and after 1000 years, it is approximately 41 m thick. Even after 1000 years, the concentration of SO_2 in a large portion of the center of the cone remains unchanged.

The effective flux of SO_2 from the entire cone over time is shown in Figure 6a for depths of 0.8 and 2.4 km. Initially, the flux of SO_2 into the bulk brine is limited mostly by solubility, and later, the thick zone of depletion acts as a barrier for diffusion. For both *PT* conditions, after the first 200 years, the flux is two orders of magnitude less than the flux during the initial years. If the model allowed for SO_2 to accumulate in the bulk brine, the flux of SO_2 from the cone would be even slower (see Ellis et al. (*8*)). Slower flux would also be predicted in the case of a model that described SO_2 partitioning to a residual brine phase within the $scCO_2$ cone.

Figure 6b shows the total amount of SO_2 that remains in the cone over time. Even though the effective flux in the case of 5% SO_2 is consistently five times larger than the effective flux for the 1% case (Figure 6a), this difference has a negligible effect on the percent of SO_2 remaining. In the first few years, nearly 5% of the SO_2 leaves the cone. After this, there is a more gradual change in the percent of SO_2 removed because of a slower flux of SO_2 from the cone during these years. After 1000 years, 64−75% of SO_2 still remains in the cone for all of the *PT* conditions simulated.

The variation in flux with depth seen in Figure 6 is due to the variation in the diffusion coefficient of SO_2 in $scCO_2$. For 1% SO_2, at 0.8 km, the diffusion coefficient is 4.76×10^{-8} m^2/sec, compared with 1.9×10^{-8} m^2/sec for the 2.4 km depth, both with error of ±7% (see Supporting Information). As shown in Figure S-1 in the Supporting Information, at shallower depths, there is little change in $D_{SO2,CO2}$ with temperature, and values are quite sensitive to changes in pressure. A pressure increase from 80 bar to only 100 bar produces a decrease in $D_{SO2,CO2}$ from 6×10^{-8} to 3×10^{-8} m^2/sec. At greater depths, $D_{SO2,CO2}$ values decrease slightly with pressure, and the increase with temperature is more substantial than at shallower depths. The balance of these two effects means that, for depths of 1.2−2.4 km, the $D_{SO2,CO2}$ contours align with the *PT* gradient such that there is little change in $D_{SO2,CO2}$ values.

Implications for Geologic CO_2 Sequestration. As mentioned in the Introduction, prior co-injection modeling studies predicted low pH conditions because of the formation of sulfur-containing acids and that these conditions would be sustained for decades. It is certainly the case that SO_2 is

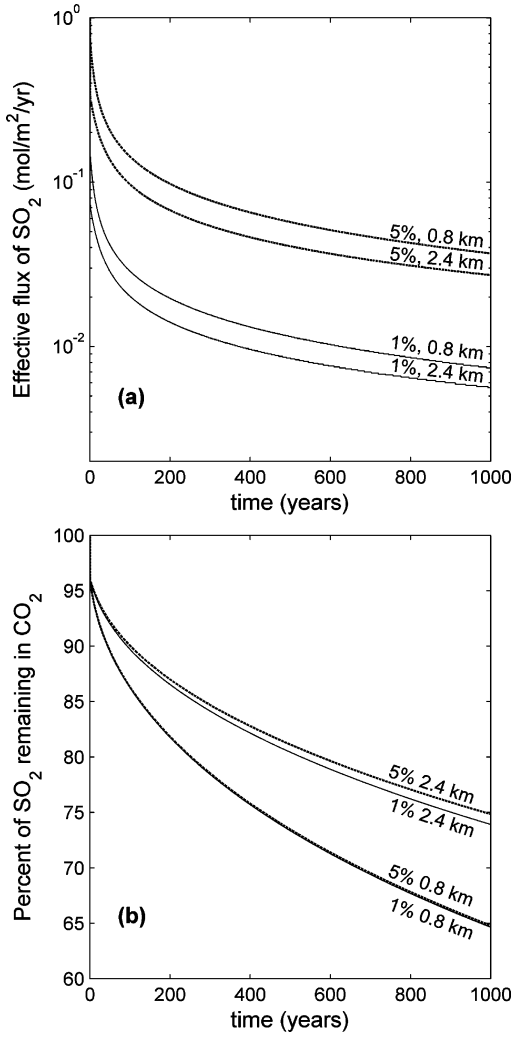

FIGURE 6. (a) Effective flux of SO_2 from $scCO_2$ cone and (b) percent of SO_2 remaining in the cone for 1 and 5% SO_2 at depths of 0.8 and 2.4 km.

very soluble and much more soluble than CO_2. However, our results show that SO_2 solubility decreases substantially with depth. By not accounting for changes in K_H and ϕ with depth, the partitioning of SO_2 would be overestimated by more than an order of magnitude at depths of 2.4 km. Furthermore, if the fluids are fairly stationary for long time periods, conditions that would not favor mixing of the brine and $scCO_2$, diffusion limitations may significantly limit the extent of SO_2 mass transfer to the bulk brine. This would limit the formation of sulfur-containing acids and their impact on brine pH. This finding is very different from the conclusions presented in other studies. Of course, reality is represented neither by the perfectly mixed phase-equilibrium scenario of previous studies nor by the perfectly stagnant diffusion-limited scenario modeled here. Reality lies somewhere between these two extremes, in which some degree of mixing will occur and some degree of transport limitations will exist. This work has demonstrated the important role of such transport limitations in governing the fate of co-injected SO_2. Future reactive transport studies should account for the possibility of diffusion-limited release of SO_2 from the $scCO_2$ phase. Some of these effects are discussed in Ellis et al. 2009 (*8*) who considered a variety of reaction and transport scenarios to estimate the potential for brine acidification from SO_2 fluxes.

Acknowledgments

Financial support for this project came from the Department of Energy, Office of Basic Energy Sciences, through Grant no. DE-FG02-05ER15636.

Supporting Information Available

Supporting Information includes sedimentary basin *PT* gradients, data used to estimate Henry's Law constants and mixture properties, *PT* contour plot of adjusted Henry's Law constants for SO_2, derivation of the diffusion model equations, diffusion coefficients for SO_2 in $scCO_2$ and error propagation for calculations of Henry's law constant, mixture density, and the diffusion coefficient. This material is available free of charge via the Internet at http://pubs.acs.org.

Literature Cited

(1) Bruant, R. G.; Guswa, A. J.; Celia, M. A.; Peters, C. A. Safe storage for CO_2 in deep saline aquifers. *Environ. Sci. Technol.* **2002**, *26* (11), 240a–245a.

(2) Benson, S. M.; Cole, D. R. CO_2 sequestration in deep sedimentary formations. *Elements.* **2008**, *4* (5), 325–331.

(3) Metz, B.; Davidson, O.; de Coninck, H.; Loos, M.; Meyer, L. *Carbon Dioxide Capture and Storage*; IPCC: Cambridge, England, 2005.

(4) U.S. Environmental Protection Agency *Acid Rain and Related Programs 2007 Progress Report*; EPA: Washington, DC, 2009.

(5) Chestnut, L. G.; Mills, D. M. A fresh look at the benefits and costs of the US acid rain program. *J. Environ. Manage.* **2005**, *77* (3), 252–266.

(6) Pollak, M. F.; Wilson, E. J. Regulating geologic sequestration in the united states: early rules take divergent approaches. *Environ. Sci. Technol.* **2009**, *43* (9), 3035–3041.

(7) Gale, J. Impure thoughts. *Int. J. Greenhouse Gas Control* **2008**, (3), 1–2.

(8) Ellis, B. R.; Crandell, L. E.; Peters, C. A. Limitations for brine acidification due to SO_2 co-injection in geologic carbon sequestration *Int. J. Greenhouse Gas Control* **2009**, DOI 10.1016/j.ijggc.2009.11.006.

(9) Gaus, I. M.; Azaroual, M.; Czernichowski-Lauriol, I. Reactive transport modeling of the impact of CO_2 injection on the clayey cap rock at Sleipner (North Sea). *Chem. Geol.* **2005**, *217* (3−4), 319–337.

(10) Rochelle, C. A.; Czernichowski-Lauriol, I.; Milodowski, A. E. *The impact of chemical reactions of CO_2 storage in geological formations: a brief review.* Special Publications. Geological Society: London, 2004; pp 87−106.

(11) Gunter, W. D.; Perkins, E. H.; Hutcheon, I. Aquifer disposal of acid gases: modeling of water-rock reactions for trapping of acid wastes. *Appl. Geochem.* **2000**, *15* (8), 1085–1095.

(12) Kutchko, B. G.; Strazisar, B. R.; Dzombak, D. A.; Lowry, G. V.; Thaulow, N. Degradation of well cement by CO_2 under geologic sequestration conditions. *Environ. Sci. Technol.* **2007**, *41* (13), 4787–4792.

(13) Peters, C. A. Accessibilities of reactive minerals in consolidated sedimentary rock: An imaging study of three sandstones. *Chem. Geol.* **2009**, *265*, 198–208.

(14) Bennion, B.; Bachu, S. Drainage and imbibition relative permeability relationships for supercritical CO_2/brine and H_2S/brine systems in intergranular sandstone, carbonate, shale, and anhydrite rocks. *Spe. Reservoir Evaluation Eng.* **2008**, *11* (3), 487–496.

(15) Knauss, K. G.; Johnson, J. W.; Steefel, C. I. Evaluation of the impact of CO_2, co-contaminant gas, aqueous fluid and reservoir rock interactions on the geologic sequestration of CO_2. *Chem. Geol.* **2005**, *217* (3−4), 339–350.

(16) Xu, T. F.; Apps, J. A.; Pruess, K.; Yamamoto, H. Numerical modeling of injection and mineral trapping of CO_2 with H_2S and SO_2 in a sandstone formation. *Chem. Geol.* **2007**, *242* (3−4), 319–346.

(17) Bachu, S.; Adams, J. J. Sequestration of CO_2 in geological media in response to climate change: capacity of deep saline aquifers to sequester CO_2 in solution. *Energy Convers. Manage.* **2003**, *44* (20), 3151–3175.

(18) Duan, Z. H.; Sun, R. An improved model calculating CO_2 solubility in pure water and aqueous NaCl solutions from 273 to 533 K and from 0 to 2000 bar. *Chem. Geol.* **2003**, *193* (3−4), 257–271.

(19) Portier, S.; Rochelle, C. Modeling CO_2 solubility in pure water and NaCl-type waters from 0 to 300 degrees C and from 1 to 300 bar - application to the Utsira formation at Sleipner. *Chem. Geol.* **2005**, *217* (3−4), 187–199.
(20) Bachu, S. Screening and ranking of sedimentary basins for sequestration of CO_2 in geological media in response to climate change. *Environ. Geol.* **2003**, *44* (3), 277–289.
(21) Rabe, A. E.; Harris, J. F. Vapor liquid equilibrium data for the binary system, sulfur dioxide and water. *J. Chem. Eng. Data* **1963**, *8* (3), 333–336.
(22) Rumpf, B.; Maurer, G. Solubilities of hydrogen cyanide and sulfur dioxide in water at temperatures from 293.15 to 413.15 K and pressures up to 2.5 MPa. *Fluid Phase Equilib.* **1992**, *81*, 241–260.
(23) Hocking, M. B.; Lee, G. W. Calculated sulfur-dioxide equilibria at low concentrations between air and water. *Water Air Soil Pollut.* **1977**, *8* (3), 255–262.
(24) Rodriguez-Sevilla, J.; Alvarez, M.; Liminana, G.; Diaz, M. C. Dilute SO_2 absorption equilibria in aqueous HCl and NaCl solutions at 298.15 K. *J. Chem. Eng. Data* **2002**, *47* (6), 1339–1345.
(25) Millero, F. J.; Hershey, J. P.; Johnson, G.; Zhang, J. Z. The solubility of SO_2 and the dissociation of H_2SO_3 in NaCl solutions. *J. Atmos. Chem.* **1989**, *8* (4), 377–389.
(26) Xia, J. Z.; Rumpf, B.; Maurer, G. The solubility of sulfur dioxide in aqueous solutions of sodium chloride and ammonium chloride in the temperature range from 313 to 393 K at pressures up to 3.7 MPa: experimental results and comparison with correlations. *Fluid Phase Equilib.* **1999**, *165* (1), 99–119.
(27) Weisenberger, S.; Schumpe, A. Estimation of gas solubilities in salt solutions at temperatures from 273 to 363 K. *AIChE J.* **1996**, *42* (1), 298–300.
(28) Pereda, S.; Thomsen, K.; Rasmussen, P. Vapor-liquid-solid equilibria of sulfur dioxide in aqueous electrolyte solutions. *Chem. Eng. Sci.* **2000**, *55* (14), 2663–2671.
(29) Andreasen, A.; Mayer, S. Use of seawater scrubbing for SO_2 removal from marine engine exhaust gas. *Energy Fuels* **2007**, *21* (6), 3274–3279.
(30) Lee, B. I.; Kesler, M. G. A generalized thermodynamic correlation based on three-parameter corresponding states. *AIChE J.* **1975**, *21* (3), 510–527.
(31) Yang, J.; Griffiths, P. R.; Goodwin, A. R. H. Comparison of methods for calculating thermodynamic properties of binary mixtures in the sub and super critical state: Lee-Kesler and cubic equations of state for binary mixtures containing either CO_2 or H_2S. *J. Chem. Thermodyn.* **2003**, *35*, 1521–1539.
(32) Lemmon, E. W.; Span, R. Short fundamental equations of state for 20 industrial fluids. *J. Chem. Eng. Data* **2006**, *51*, 795–850.
(33) Sander, R. Henry's Law Constants, in *NIST Chemistry WebBook, NIST Standard Reference Database Number 69*, Lindstrom, P. J.; Mallard, W. G., Eds.; Thermodynamics Research Center N.B.L.: Gaithersburg, MD.
(34) Thermodynamics Source Database. In *NIST Chemistry WebBook, NIST Standard Reference Database Number 69*; Lindstrom, P. J., Mallard, W. G., Eds.; National Institute of Standards and Technology: Gaithersburg, MD.
(35) McPherson, B. J. O. L.; Han, W. S.; Cole, B. S. Two equations of state assembled for basic analysis of multiphase CO_2 flow and in deep sedimentary basin conditions. *Comput. Geosci.* **2008**, *34* (5), 427–444.
(36) Bachu, S. Sequestration of CO_2 in geological media: criteria and approach for site selection in response to climate change. *Energy Convers. Manage.* **2000**, *41* (9), 953–970.
(37) van der Meer, L. G. H. The conditions limiting CO_2 storage in aquifers. *Energy Convers. Manage.* **1993**, *34* (9−11), 959–966.
(38) Prausnitz, J. M.; Lichtenthaler, R. N.; de Azevedo, E. G. *Molecular Thermodynamics of Fluid-Phase Equilibria*, 2nd ed.; Prentice-Hall, Inc.: Eaglewood Cliffs, NJ, 1986.
(39) Brelvi, S. W.; O'Connell, J. P. Corresponding states correlations for liquid compressibility and partial molal volumes of gases at infinite dilution in liquids. *AIChE J.* **1972**, *18* (6), 1239–1243.
(40) Tarakad, R. R.; Danner, R. P. Improved corresponding states method for polar fluids - correlation of 2nd virial-coefficients. *AIChE J.* **1977**, *23* (5), 685–695.
(41) Reid, R. C.; Prausnitz, J.M.; Poling, B. E. *The Properties of Gases and Liquids*, 4th ed.; McGraw-Hill Companies, 1987.
(42) Doughty, C.; Pruess, K. Modeling supercritical carbon dioxide injection in heterogeneous porous media. *Soil Sci. Soc. Amer.* **2004**, *3* (3), 837–847.
(43) Bickle, M.; Chadwick, A.; Huppert, H. E.; Hallworth, M.; Lyle, S. Modeling carbon dioxide accumulation at Sleipner: Implications for underground carbon storage. *Earth Planet. Sci. Letters* **2007**, *255* (1−2), 164–176.
(44) Nordbotten, J. M.; Celia, M. A. Similarity solutions for fluid injection into confined aquifers. *J. Fluid Mech.* **2006**, *561*, 307–327.
(45) Bachu, S.; Gunter, W. D.; Perkins, E. H. Aquifer disposal of CO_2 - hydrodynamic and mineral trapping. *Energy Convers. Manage.* **1994**, *35* (4), 269–279.
(46) Wilson, M.; Monea, M. IEA GHG Weyburn CO_2 Monitoring and Storage Project Summary Report 2000−2004 *7th International Conference on Greenhouse Gas Technologies*; Petroleum Technology Research Centre: Vancouver, Canada, 2004.
(47) Cussler, E. L. *Diffusion Mass Transfer in Fluid Systems*, 3rd ed. 3rd ed.; Cambridge University Press: New York, 2009.
(48) Span, R.; Wagner, W. A new equation of state for carbon dioxide covering the fluid region from the triple-point temperature to 1100 K at pressures up to 800 MPa. *J. Phys. Chem. Ref. Data* **1996**, *25* (6), 1509–1596.
(49) Ihmels, E. C.; Lemmon, E. W.; Gmehling, J. An equation of state and compressed liquid and supercritical densities for sulfur dioxide. *Fluid Phase Equilib.* **2003**, *207* (1−2), 111–130.
(50) Oldenburg, C. M., Migration mechanisms and potential impacts of CO_2 leakage and seepage. In *Carbon Capture and Sequestration: Integrating Technology, Monitoring and Regulation*. Wilson, E. J., Gerard, D., Eds.; Blackwell Publishing, 2007.

ES902612M